Supplementary Note 1 CdSe QDs were dissolved in deuterated toluene to give a volume of 39.8 μL. This was transferred to the NMR probe with 0.2 μL of benzene as an internal standard. The population of core CdSe QDs was calculated using the empirical relations of Jasieniak *et al*.[1] The total number of QDs in the NMR probe was determined using the Avogadro constant (2.16x10^{15} QDs). The number of moles of ligand was calculated as follows.

Total benzene integral = 0.46

Integral per proton

$$\frac{0.046}{6} = 0.076 \tag{1}$$

where the density of benzene is $\rho = 0.87\ \mathrm{g\ cm^{-3}}$ and a volume of $0.2\ \mu\mathrm{L}$ was used. Hence, we calculate the total number of moles of benzene used to be $2.2\ \mu\mathrm{mol}$.

To identify the ligand identities we performed simple 1D proton NMR on octadecylamine (ODA), stearic acid (SA) and trioctylphosphine (TOP). The isolated free SA molecule exhibits a triplet peak (alpha carbon protons) at 2.03 ppm buried next to the deuterated toluene signal (Supplementary Figure 2). This was absent in the spectra of the QDs, which suggest SA may be absent. Of course, we cannot rule out the presence of the bound SA from this simple comparison due to spectral broadening of the SA at the QD surface and so we employed XPS elemental analysis. Fortuitously, each ligand (SA, ODA and TOP) exhibits a unique XPS signal (oxygen, nitrogen and phosphorus) respectively. The XPS measurements (Supplementary Figure 3) show the presence of oxygen and the absence of nitrogen and phosphorus signals. Hence, XPS data suggests a surface dominated by the SA. This was further probed using NMR.

Attention is now turned to the NMR. We make use of the integral areas to deconvolute any spectral overlap. We find for our QD NMR sample a small peak at 1.95 ppm, which may be attributed to residual non-coordinating ODE (Supplementary Figure 2) remaining from the QD synthesis. The ODE molecule is expected to produce a strong signal at about 1.2 ppm for the carbon backbone protons and a triplet signal at about 0.9 ppm for the terminal methyl protons. The peak areas are predicted to be in a ratio of 2:28:3 for the signals at 1.95, 1.2 and 0.9 ppm respectively. Integration of the peak at 1.95 ppm yields a value of 0.034, where the areas for the carbon backbone protons and methyl protons are then

$$\frac{0.035}{2} \times 28 = 0.49 \tag{2}$$

$$\frac{0.035}{2} \times 3 = 0.053 \tag{3}$$

these calculated peak areas must be subtracted from the areas calculated for both the carbon backbone protons and methyl protons to produce the correct areas for the free ligand in our QD sample. The corrected areas are thus

$$0.48 - 0.49 = -0.01 \quad (4)$$

$$0.066 - 0.053 = 0.013 \quad (5)$$

hence, we find the alkyl and methyl integrals are dominated by non-coordinating ODE and for simplicity, we assume that free ligand is negligible for the remaining calculations. The broad shoulders of the alkyl backbone and methyl signals are thus exclusively bound ligand for the QD samples. The ratio between the broad carbon backbone proton signals (1.4 ppm) and broad bound methyl protons (0.95 ppm) is measured as

$$\frac{0.24}{0.024} = 10.0 \quad (6)$$

where for the pure ligand we calculate an expected alkyl backbone (30 H) to methyl proton (3 H) ratio of

$$\frac{30}{3} = 10.0 \text{ SA} \quad (7)$$

As discussed earlier, the alpha carbons of the SA appear downfield (2.03 ppm) from the remainder of the alkyl chain and do not contribute to the bound backbone integral area $(32 - 2) = 30$ H. From the above ratio, we can deduce that the surface is dominated by SA, which corroborates data obtained from XPS. If a fraction of TOP ligands were present, we would expect to experimentally observe a backbone:methyl ratio intermediate of pure TOP (14/3) 4.67 and pure SA (30/3) 10.0. For the aliphatic linear chain methyl resonance of the QD sample we calculate

$$\frac{0.024}{3} = 0.008 \quad (8)$$

$$\frac{0.076}{0.008} = 9.5 \quad (9)$$

$$\frac{2.2 \times 10^{-6}}{9.5} = 2.32 \times 10^{-7} \text{ mol} \quad (10)$$

where we have 1.39× 10^{17} linear aliphatic SA molecules.

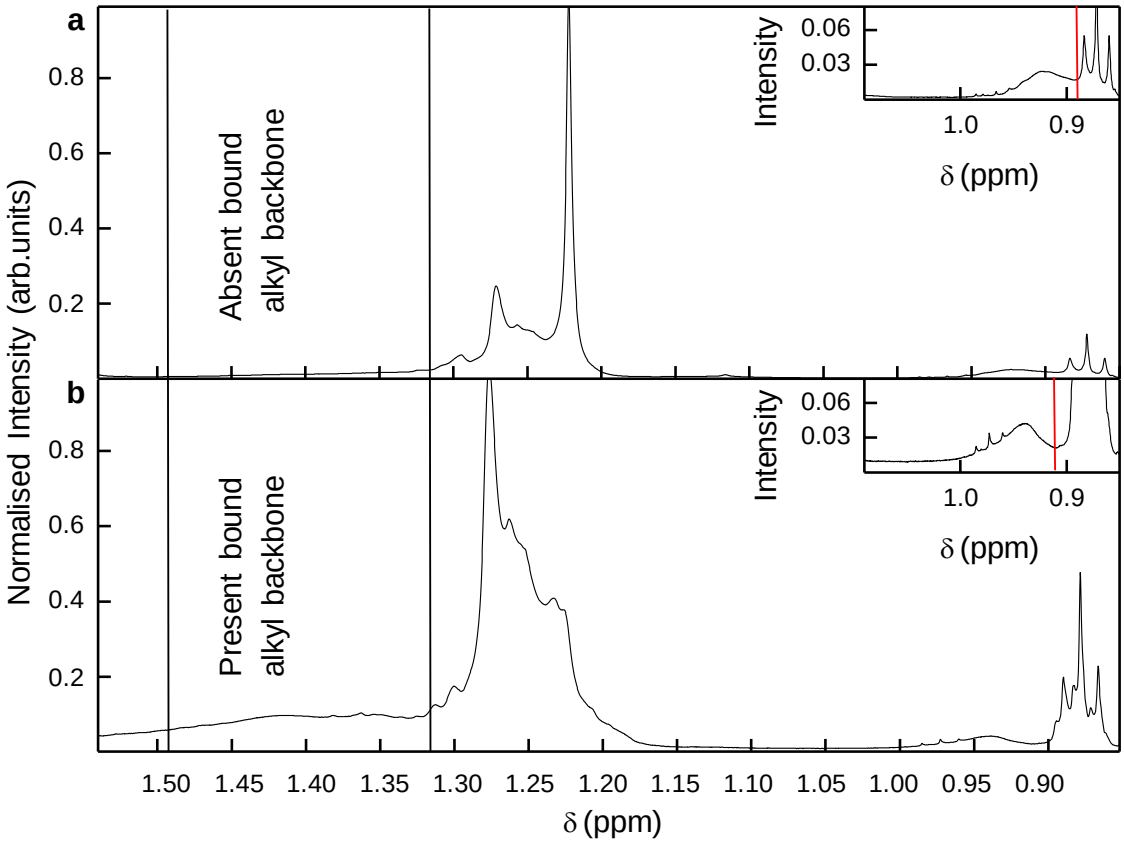

Supplementary Figure 1 Static solution NMR spectrum versus HR-MAS. **a** static solution NMR showing the important methyl and alkyl backbone signals at 0.9 and 1.2-1.3 ppm, respectively. The slowly tumbling bound ligand undergoes extreme spectral broadening for the alkyl backbone and is lost in the baseline. The inset shows the methyl resonance in greater detail. The red line shows the turning point (0.89 ppm) between the sharp resolved triplet and broad bound signal. **b** HR-MAS spectrum of the QD solution. Spectral broadening is reduced for the alkyl backbone signal compared with the static solution spectrum. Inset shows the peak separation for the methyl signal is improved under MAS, where the turning point (0.91 ppm)(red line) permits improved integration accuracy relative to the static solution spectrum.

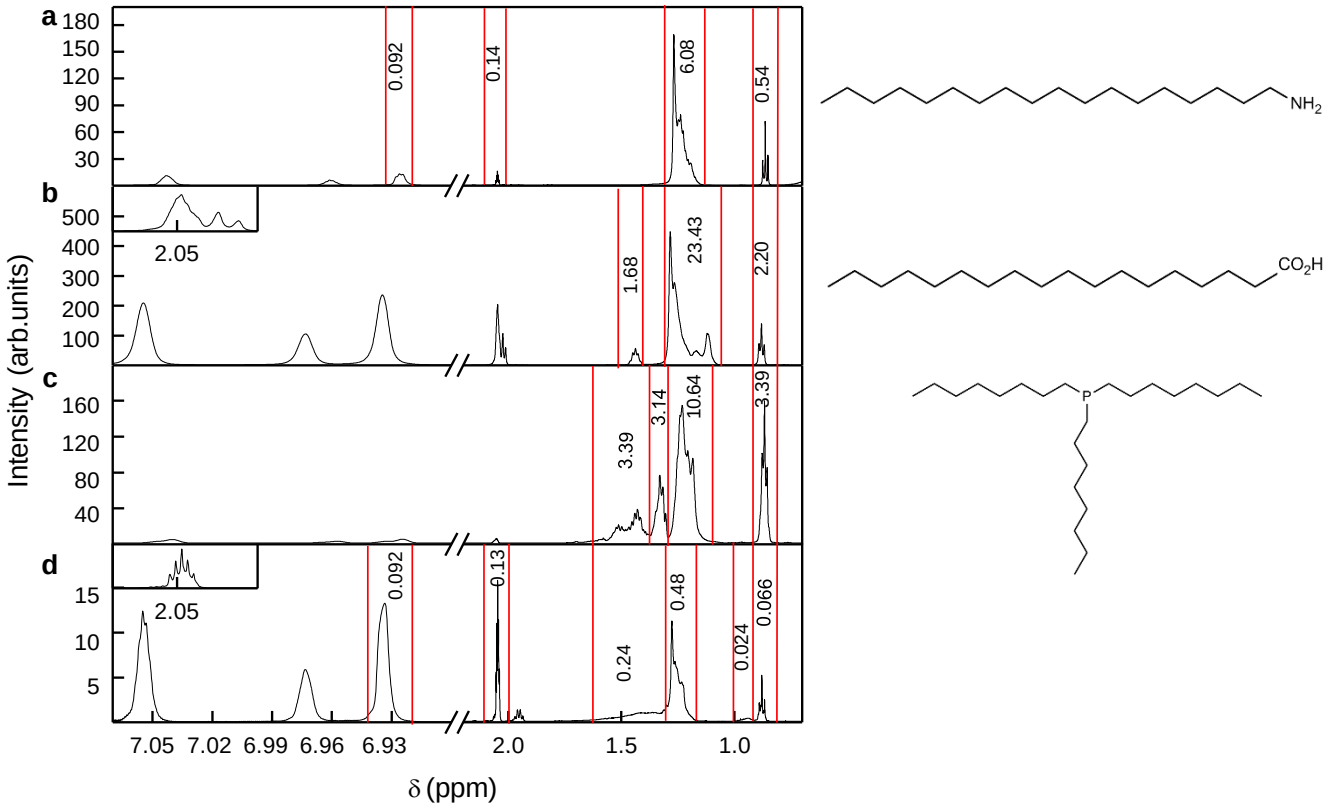

Supplementary Figure 2 1D proton NMR spectra of isolated free ligand and QD/ligand samples dissolved in deuterated toluene. The red lines highlight the integral region, where the numerical integral values are presented between the red integral boundaries. **a** isolated free ODA ligand which exhibits a methyl resonance at about 0.9 ppm and CH_2 backbone at 1.2 ppm. The peaks at 2.05, 6.93, 6.97 and 7.06 all belong to the deuterated toluene. **b** NMR spectra of stearic acid. The methyl resonance is found at 0.9 ppm and the bulk of the CH_2 backbone at 1.2 ppm. The multiplet peak at 1.48 ppm arises from the beta carbon protons. Importantly, the alpha carbon proton triplet appears at 2.03 ppm and is merged with the deuterated toluene signal (see inset). **c** proton NMR of free TOP. The methyl signal appears at 0.9 ppm, where the bulk of the CH_2 backbone appears at 1.2 ppm. The downfield signals at 1.34 and 1.49 arise from the beta and alpha carbons respectively. **d** QD bound/free ligand sample. The broad downfield shoulders of the methyl and CH_2 backbone represent the bound fraction. Interestingly, the signal at 2.05 ppm (inset) shows no evidence of the stearic acid triplet probably due to spectral broadening.

Supplementary Note 2

The density of a single CdSe QD was estimated from x-ray diffraction data (Supplementary Figure 4) according to the following

$$\rho_{\mathrm{CdSe}} = \frac{4(\mathrm{Se}) + 4(\mathrm{Cd})}{a^3} \tag{11}$$

where ρ_{CdSe} is the density of a single CdSe QD, (Se) and (Cd) represent the weight of single selenium and cadmium atoms, respectively and a is the lattice constant. The density was estimated to be 5.66 g cm^{-3}. The total number of CdSe ion pairs for a single QD was subsequently calculated using the following relation

$$\frac{V_{\mathrm{QD}}\rho_{\mathrm{CdSe}}}{M_{r\mathrm{CdSe}}}N_A = 249\ \mathrm{CdSe\ Ion\ Pairs} \tag{12}$$

where V_{QD} is the volume of a single QD, the density of the QD is given by ρ_{CdSe}, the molecular weight is $M_{r\mathrm{CdSe}}$ and N_{A} is the Avogadro constant. The QD volume was approximated assuming the QD to be perfectly spherical. HR-TEM measurements of core CdSe indicate 1.5 nm radii. Hence, V_{QD} was calculated from

$$V_{QD} = \frac{4}{3}\pi r^3 \tag{13}$$

where r is the QD radii as measured from HR-TEM. Following calculation of the total number of CdSe ion pairs, a simple spherical cluster approximation was used to determine the number of surface atoms for a single QD. Ultimately, for a QD which consists of almost 500 atoms, 45% of the total atoms exist at the QD surface. Hence, the QD surface presents about 225 atoms in total, where if one assumes a 1:1 = Cd:Se stoichiometry as measured by ICP-MS (Supplementary Figure 6), then surface cadmium sites are on the order of 112 per QD.

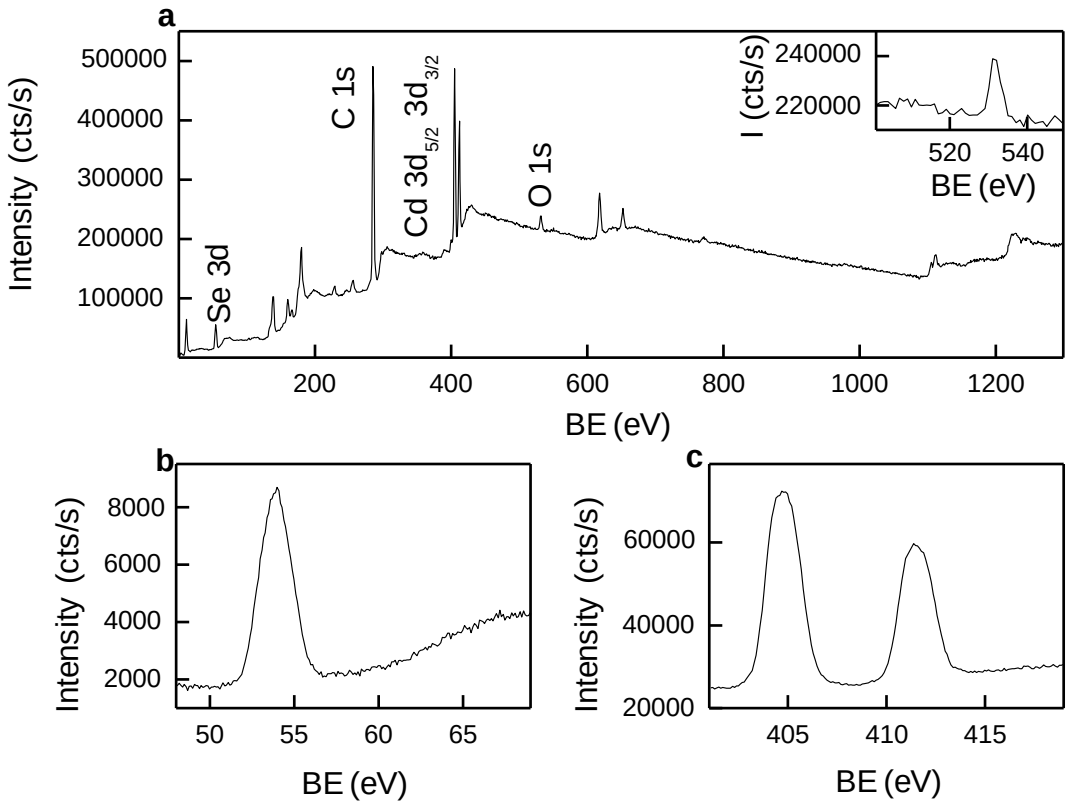

Supplementary Figure 3 XPS spectra of as-prepared QDs. **a** survey scan over a broad range of binding energies (BE). There is no peak at 130 or 399 eV indicating the absence of phosphorus and nitrogen in our samples. The closest peak to the expected phosphorus binding energy is at 137 eV and may be attributed to a selenium Auger electron. A small oxygen signal is present at 531 eV. The inset shows the oxygen 1s signal in greater detail. **b** and **c** show detailed scans of the selenium 3d and cadmium $3d_{5/2}$ and $3d_{3/2}$ binding energies, respectively.

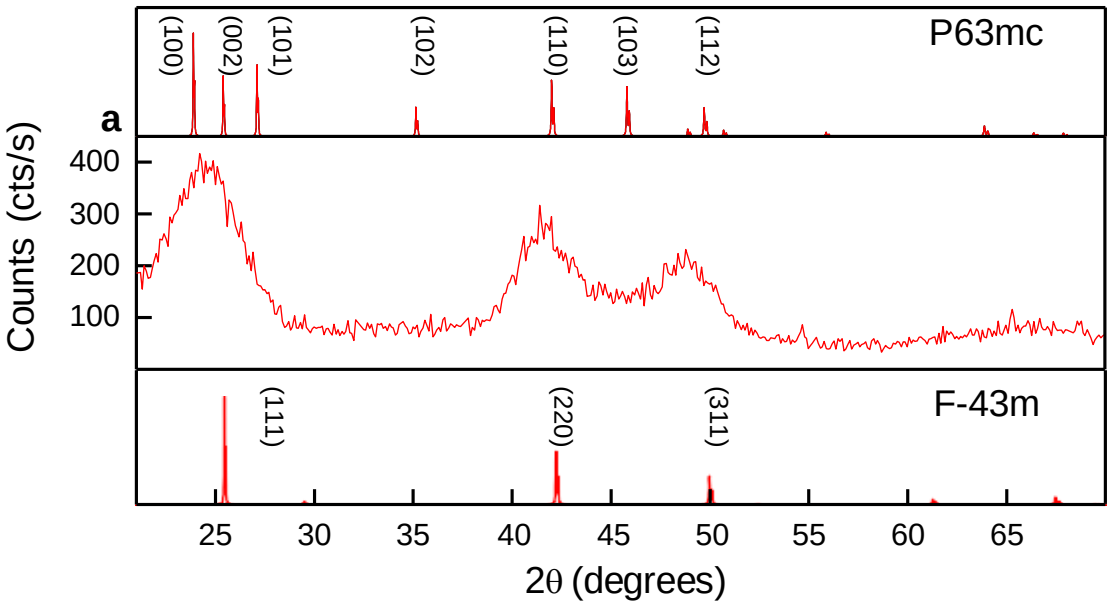

Supplementary Figure 4 XRD pattern of as-prepared CdSe QDs with corresponding stick patterns of both the wurtzite P63mc phase and the zinc blende F-43m polymorph. **a** XRD diffractogram of CdSe QDs. The peaks are broadened due to the nanocrystalline nature of the sample. The absence of the (102) and (103) reflections suggest the QDs adopt the zinc-blende phase in this case. The use of HR-TEM in the main text assists with the assignment of the lattice structure. Importantly, crystallographic assignment permits calculation of QD density and hence the number of surface atoms for a single QD.

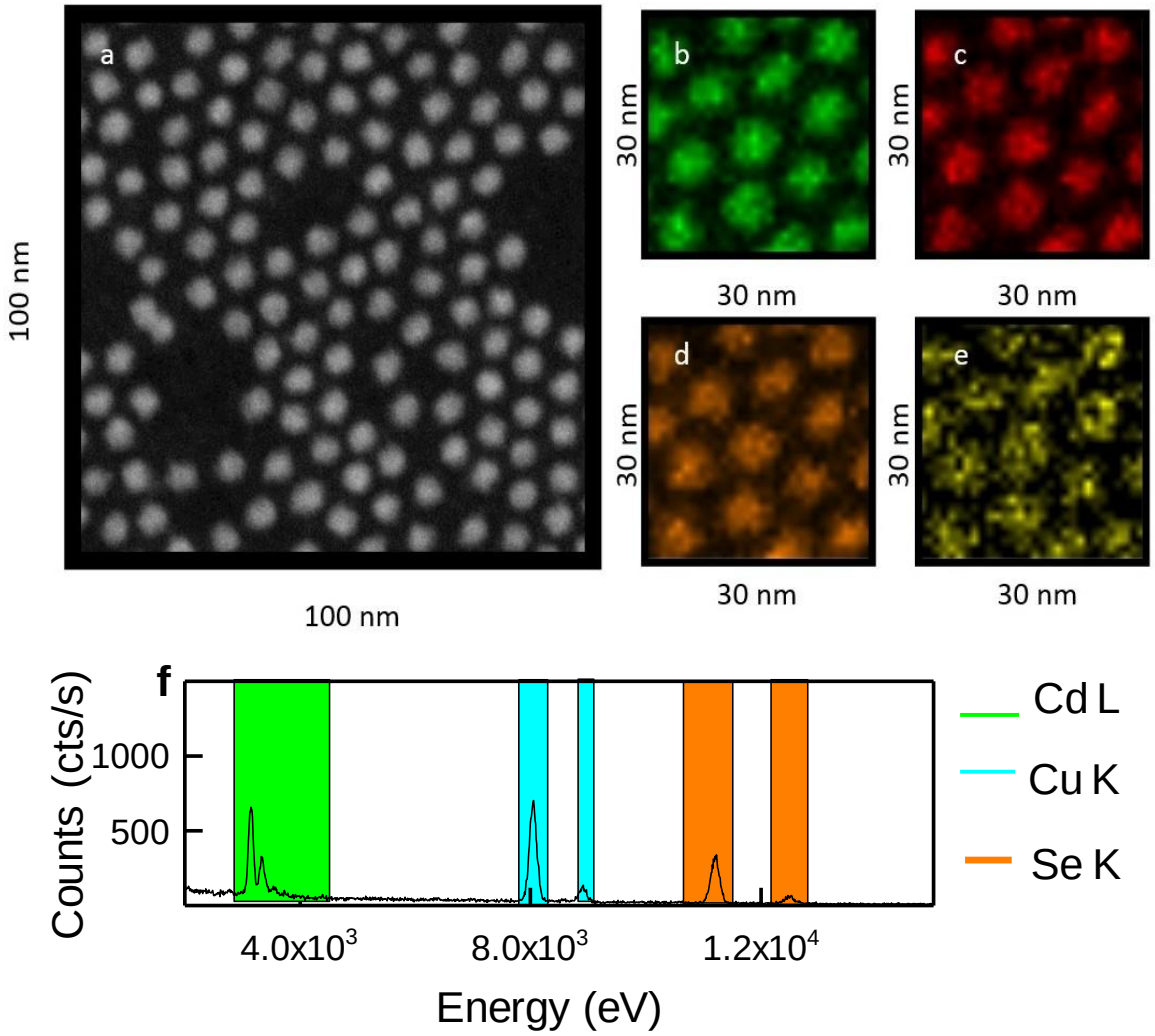

Supplementary Figure 5 Scanning transmission electron microscopy-energy dispersive x-rays (STEM-EDX) and high angle annular dark field (HAADF) images of the as-synthesised CdSe QDs. **a** HAADF image of a large area of QDs. The QDs used in the studies reported had a diameter of approximately 3 nm. **b**, **c**, **d** and **e** spectrum images of CdSe QDs. Here green highlights the Cd L-alpha lines, red the Cd L-beta lines, orange the Se K-alpha lines and yellow the Se K-beta lines. **f** raw EDX spectrum collected from the CdSe QDs. A colour key is provided on the right of the graph. The copper signal arises from the carbon/copper grids used.

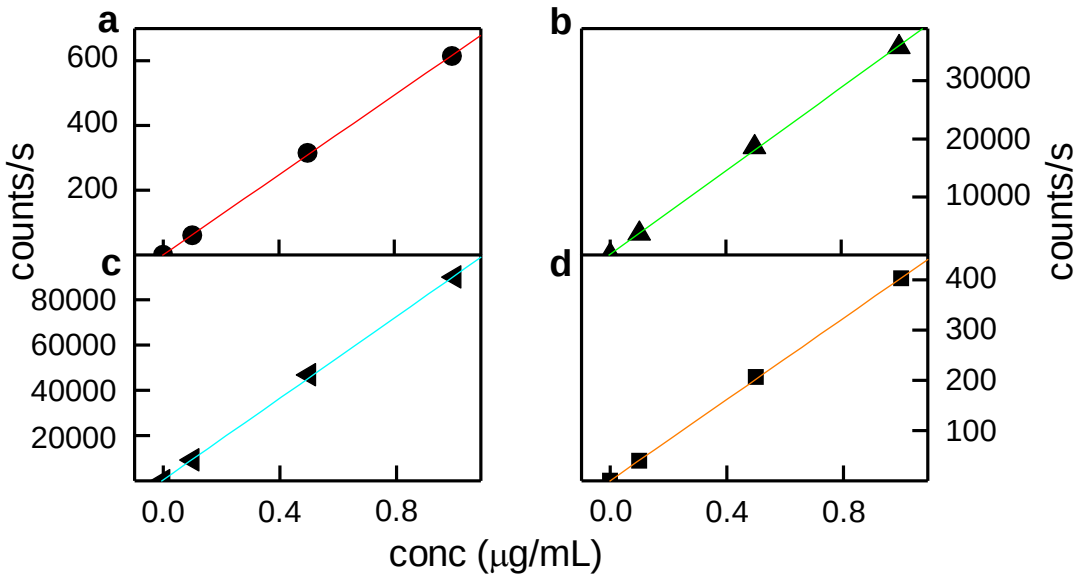

Supplementary Figure 6 Inductively coupled plasma mass spectroscopy (ICP-MS) calibration and identification of crystal stoichiometry. **a**, **b**, **c** and **d** calibration curves using ICP-MS standards of Se^{82}, Cd^{114}, Cd^{111} and Se^{77}, respectively. It was found that the crystals exhibit a near-binary stoichiometry (1.08:1 = Cd:Se), which is in good agreement with the literature. For simplicity, a 1:1 = Cd:Se ratio was subsequently used, in the main text, to estimate the number of surface cadmium sites. Importantly, the inclusion factor, in the main text, was approximated from ligand density NMR studies and the availability of surface cadmium sites, which were calculated using both XRD and ICP-MS measurement of QD stoichiometry.

Supplementary Note 3 In the CTST model, radiative recombination of the neutral, exciton-state, X_{00} competes with tunnelling of the electron from the conduction band-edge of the QD to an external trap [2]. A tunnelling event leaves the QD charged and subsequent excitation generates either the core-charged off-state, X^{+}_{10}, made dark by effective Auger quenching of the core-trion or the surface-charged on-state, X^{+}_{01}, made bright by a probability of hole-trapping at the QD-surface (area dependent) and neutralisation of the core-exciton. The duration of PL-on and off-times is determined by the tunnelling rate of the electron from the external trap to either the surface-stabilised hole in the X^{+}_{01} state or core-hole in the X^{+}_{10} state at the valence band-edge of the QD, respectively. The tunnelling rates depend on a capture cross-section, but also crucially the tunnelling probability, which has a $e^{-\sqrt{V-E}\,l}$ dependence on the potential barrier V and particle kinetic energy E (in eV) and tunnelling length l (in Å). Within the CTST framework the mean tunnelling barriers for electron recombination at the QD are given by[2]

$$V_{\mathrm{off}}^{-} = E_{\mathrm{ea}} - \frac{E_{\mathrm{QD}}}{2} + \frac{3}{2}\phi_{\mathrm{e}} \tag{14}$$

$$V_{\mathrm{on}}^{-} = V_{\mathrm{off}}^{-} + \phi_{\mathrm{h}}/2 \tag{15}$$

where E_{ea} and E_{QD} are the electron affinity and band-gap energy of the QD and ϕ_{e} and ϕ_{h} and the self-energies of the electron and hole, respectively. For the electron stabilised in the ligand-host of effective dielectric constant $\varepsilon_{\mathrm{eff}}$, far from the QD ($l = 1 - 2$ nm) the self-trap energies are given (in Gaussian units) by

$$\phi_{\mathrm{e}} = \frac{e^2}{2r}\left(1 - \frac{1}{\varepsilon_{\mathrm{eff}}}\right) \tag{16}$$

and for the hole stabilised at the QD surface

$$\phi_{\mathrm{h}} = \frac{e^2 K}{2r}\left(\frac{1}{\varepsilon_{\mathrm{eff}}} - \frac{1}{\varepsilon_{\mathrm{QD}}}\right) \tag{17}$$

where $\varepsilon_{\mathrm{QD}}$ is dielectric constant of the QD, $K = (\varepsilon_{\mathrm{QD}} - \varepsilon_{\mathrm{eff}})/(\varepsilon_{\mathrm{QD}} + \varepsilon_{\mathrm{eff}})$ and r is a nominal trap radius of the order of 0.3 nm[2]. Substitution then leads to a dependence of the tunnelling barrier on the effective dielectric constant of the form $A - B/\varepsilon_{\mathrm{eff}}$, where

$$A_{\mathrm{off}} = E_{\mathrm{ea}} - \frac{E_{\mathrm{QD}}}{2} + \frac{3e^2}{4r} \qquad B_{\mathrm{off}} = \frac{3e^2}{4r} \tag{18}$$

$$A_{\mathrm{on}} = A_{\mathrm{off}} - \frac{e^2 K}{4\varepsilon_{\mathrm{QD}} r} \qquad B_{\mathrm{on}} = B_{\mathrm{off}} - \frac{e^2 K}{4r} \tag{19}$$

and for $\varepsilon_{\mathrm{QD}} > \varepsilon_{\mathrm{eff}}$, K decays slowly with $\varepsilon_{\mathrm{eff}}$.

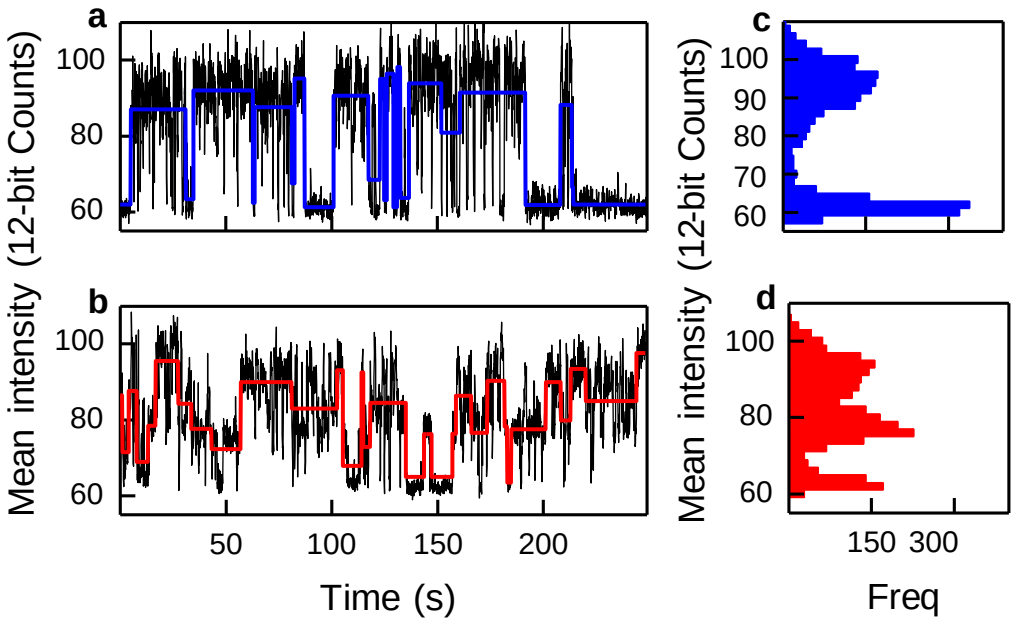

Supplementary Figure 7 Single QD emission traces. **a** trajectory trace (black line) of a single CdSe QD undergoing fluorescence intermittency. The blue line superimposed shows the results from change point analysis. The trajectory trace shown here is representative of the QDs analysed in this work. **b** single CdSe.CdS QD emission trace. Core-shell QDs were not studied in this work and serves only as a comparison to the bare CdSe QDs. The red line superimposed shows the change point analysis. **c** and **d** show the intensity histograms of bare CdSe and CdSe.CdS, respectively. Deeply modulated grey states are rare for the bare CdSe QDs and well-defined threshold separating bright and dark states can be defined. The threshold was chosen to reflect the minimum in the intensity histogram (70 counts). A deeply modulated grey state dominates for core-shell CdSe.CdS QDs. This arises naturally within the CTST model from a shift in the excess hole equilibrium toward the QD core. The blinking behaviour of core-shell QDs was not studied further in this work and for simplicity, we present our power law data in the main text as binary on and off states.

Supplementary References

1 Jasieniak, J., Smith, L., Van Embden, J., Mulvaney, P. & Califano, M. Re-examination of the size-dependent absorption properties of CdSe quantum dots. *J. Phys. Chem. C* **113**, 19468-19474 (2009).

2 Osborne, M. A. & Fisher, A. Charge-tunnelling and self-trapping: common origins for blinking, grey-state emission and photoluminescence enhancement in semiconductor quantum dots. *Nanoscale* **8**, 9272-9283 (2016).